CHEMISTRY
A EUROPEAN JOURNAL

DOI: 10.1002/chem.200902500

Photoisomerization of a Maleonitrile-Type Salen Schiff Base and Its Application in Fine-Tuning Infinite Coordination Polymers

Chun-Wei Lin,[a] Pi-Tai Chou,*[a] Yong-Hong Liao,[a] Ying-Chih Lin,*[a] Ching-Ting Chen,[a] Yu-Chun Chen,[a] Chin-Hung Lai,[a] Bo-So Chen,[a] Yi-Hung Liu,[b] Chih-Chieh Wang,[c] and Mei-Lin Ho*[c]

Abstract: Strategically designed salen ligand 2,3-bis[4-(di-*p*-tolylamino)-2-hydroxybenzylideneamino]maleonitrile (**1**), which has pronounced excited-state charge-transfer properties, shows a previously unrecognized form of photoisomerization. On electronic excitation (denoted by an asterisk), **1Z***→**1E** isomerization takes place by rotation about the C2−C3 bond, which takes on single-bond character due to the charge-transfer reaction. The isomerization takes place nonadiabatically from the excited-state (**1Z**) to the ground-state (**1E**) potential-energy surface in the singlet manifold; **1Z** and **1E** are neither thermally inconvertible at ambient temperature (25–30 °C), nor does photoinduced reverse **1E***→**1Z** (or **1Z***) isomerization occur. Isomers **1Z** and **1E** show very different coordination chemistry towards a Zn^{II} precursor. More prominent coordination chemistry is evidenced by a derivative of **1** bearing a carboxyl group, namely, *N*,*N*′-dicyanoethenebis(salicylideneimine)dicarboxylic acid (**2**). Applying **2Z** and its photoinduced isomer **2E** as building blocks, we then demonstrate remarkable differences in morphology (sphere- and needlelike nanostructure, respectively) of their infinite coordination polymers with Zn^{II}.

Keywords: isomerization • N,O ligands • photochemistry • photophysics • zinc

Introduction

Salen ligands, which are generally prepared by condensation of salicylic aldehydes and ethylenediamines, provide tetradentate coordination sites in their dianionic form and have been ubiquitously used in coordination chemistry.[1] Reports on salen ligands and their associated metal complexes are well documented, among which a variety of relevant complexes have been used for catalytic reactions, including the asymmetric ring opening of epoxides, aziridination, cyclopropanation, epoxidation of olefins,[2] cleavage of DNA, and so on.[3] Recently, salen-type transition-metal complexes have been successfully applied as emitters, and showed good stability and decent efficiency in electroluminescent (EL) devices.[4]

Of particular interest are salen ligands functionalized by an electron-donor (D)/electron-acceptor (A) pair having intramolecular charge-transfer (ICT) properties, such that the associated complexes may have nonlinear optical (NLO) properties.[5,6] To enhance the strength of ICT, the salen ligands are generally anchored by a strongly electron withdrawing moiety such as a cyano group (A) on diamines and dialkylamino substituents (D) at the conjugated position of the diamines. Such D–A–D conjugated structures have attracted much attention due to their characteristic electronic and optical properties. On excitation, substantial and symmetric intramolecular charge redistribution takes place in these D–A–D molecules, resulting in a large two-photon absorption cross section σ_2. Owing to their large electron delocalization and planar skeleton structure, further metal complexation may find great potential in view of NLO properties.[6]

[a] C.-H. Lin, Prof. P.-T. Chou, Y.-H. Liao, Prof. Y.-C. Lin, C.-T. Chen, Y.-C. Chen, Dr. C.-H. Lai, B.-S. Chen
Department of Chemistry
National Taiwan University
Taipei (Taiwan)
Fax: (+886) 2-2369-5208
E-mail: chop@ntu.edu.tw
yclin@ntu.edu.tw

[b] Dr. Y.-H. Liu
Department of Chemistry and Instrument Center
National Taiwan University, Taipei (Taiwan)

[c] Prof. C.-C. Wang, Prof. M.-H. Ho
Department of Chemistry, Soochow University, Taipei (Taiwan)
E-mail: meilin_ho@scu.edu.tw

Supporting information for this article is available on the WWW under http://dx.doi.org/10.1002/chem.200902500.

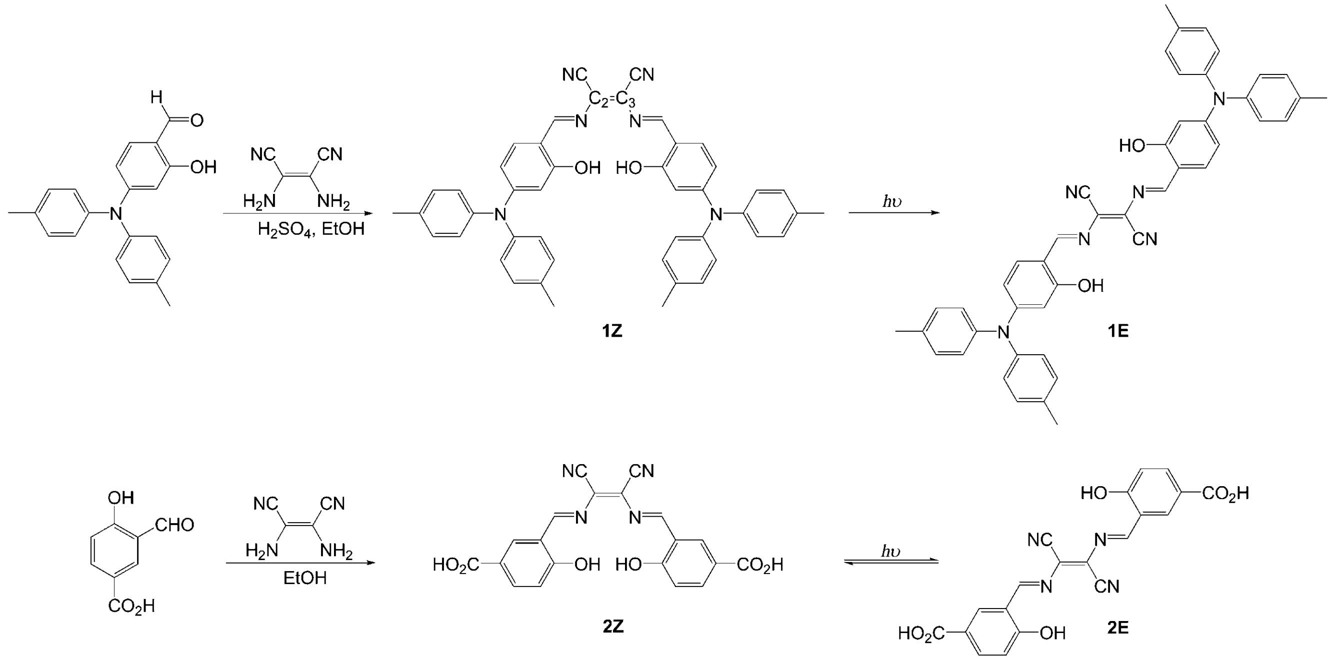

Scheme 1. Structures of and synthetic route to **1Z** and **2Z**, and their proposed photoisomers **1E** and **2E**.

To expand our long-term interest in transition metal complexes toward optoelectronic applications, we thus prepared a salen ligand by incorporating cyano and di-*p*-tolylamino substituents at designated positions, such that the resulting compound 2,3-bis[4-(di-*p*-tolylamino)-2-hydroxybenzylideneamino]maleonitrile (**1**, see Scheme 1) has prototypical D–A–D-type strong ICT in the excited state. Incorporation of a di-*p*-tolylamino instead of a dialkyl group[7] is intended to further enhance the electron-donating strength. The synthetic route seems to be straightforward, and salen compound **1** with *Z* configuration with regard to the maleonitrile C=C double bond (**1Z**, see Figure S1 in the Supporting Information) should be obtained, similar to numerous reports on salen-type ligands.[8,9]

Herein we explore a previously unrecognized feature, that is, facile photoisomerization about the maleonitrile C=C double bond of **1Z** in the excited state, forming the **1E** isomer. To further explore the differences in coordination chemistry between *E* and *Z* conformers, we then strategically designed a derivative of **1**, namely, *N*,*N*′-dicyanoethenebis(salicylideneimine) dicarboxylic acid (**2**, Scheme 1), which shares the same core moiety as **1** but has additional carboxyl functional groups. We first present the characterization and photophysical properties of **1Z** and **1E** isomers. Subsequently, photoinduced **1Z**→**1E** photoisomerization is investigated and discussed on the basis of ^{1}H NMR, UV/Vis, and fluorescence spectroscopy and theoretical approaches. With a view to applications, the coordination chemistry of **1** (*E*/*Z*) and **2** (*E*/*Z*) is then investigated. Using **2Z** and **2E** as building blocks, we then demonstrate for the first time the remarkable differences in morphology of their infinite coordination polymers with Zn^{II}.

Results and Discussion

Characterization of 1E/1Z isomers: Salen compound **1** was obtained by condensation of *cis*-diaminomaleonitrile and 2-hydroxy-4-(di-*p*-tolylamino)benzaldehyde. After filtration, the precipitate was red-brown. We then performed crystallization under room light and obtained slatelike, deep green crystals (see Table of Contents (TOC) picture, top right). Due to the *syn* addition depicted in Scheme 1, conventional wisdom leads us to propose such a Schiff base to be originally in the *Z* configuration, similar to most salen ligands reported.[8,9] To our surprise, however, as shown in Figure 1, the X-ray structural analysis unambiguously revealed the *E* configuration, in which one 4-(di-*p*-tolylamino)-2-(iminomethyl)phenol wing is rotated around the maleonitrile C=C bond and spatially aligned in a *trans* orientation with respect to the other. Except for the di-*p*-tolylamino segments, the main molecular skeleton is in a planar configuration, as indicated by the dihedral angle of about 0° between the C11-C6-C7 and C11A-C6A-C7A planes. Retention of the intramolecular hydrogen bond between O1−H and N3 (or O1A−H and N3A) is clearly indicated by the short N···O distance of 2.685 Å (2.685 Å).

To rationalize the **1E** form obtained serendipitously, we proposed that isomerization took place by thermal reaction or photoexcitation (room light) of **1Z**. We first investigated the effect of photoexcitation by performing the condensation experiment to prepare compound **1** in a more careful manner. To avoid room-light excitation, all reaction and workup procedures were performed under dim red light ($\lambda > 700$ nm), the photon energy of which is too low to be absorbed by compound **1** (vide infra). Subsequently, recrys-

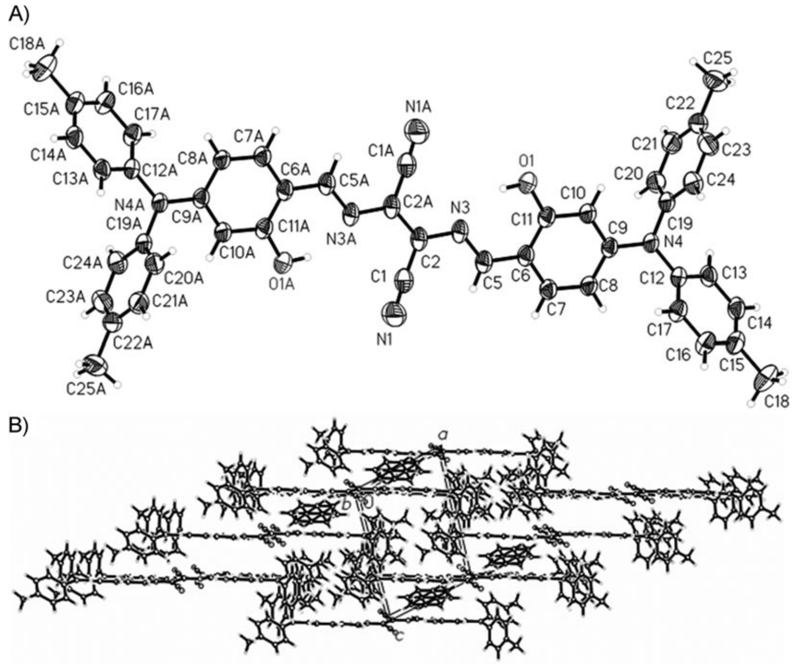

Figure 1. A) Structure of **1E** with thermal ellipsoids set at 30% probability. Selected bond lengths [Å]: C2−C2 1.377(4), C2−N3 1.382(3), N3−C5 1.309(3), C5−C6 1.418(3), C6−C7 1.410(3), C7−C8 1.366(3), C8−C9 1.407(3), N4−C9 1.388(2), N4−C12 1.430(2), N4−C19 1.441(3). Detailed data are summarized in the Supporting Information. B) Molecular arrangement of **1E** viewed along the *b* axis.

tallization was carried out in the dark at room temperature to give needlelike, brownish green crystals (TOC picture, top left). The subtle difference in morphology with respect to those obtained from the synthetic/purification route under room light might imply structural variation. In fact, as shown in Figure S1 of the Supporting Information, the X-ray analysis clearly shows a *Z* configuration, in which the two 4-(di-*p*-tolylamino)-2-(iminomethyl)phenol moieties are virtually in a *cis* configuration relative to the C2−C3 bond (see Scheme 1).

For further confirmation, ^{1}H NMR and UV/Vis absorption and emission spectra were recorded for both **1Z** and **1E**. As shown in Figure 2, although the ^{1}H NMR signals ascribed to the aromatic protons are complicated and hence may not be convincing enough to differentiate **1Z** and **1E**, they are readily distinguishable for both imine protons (**1E**: $\delta=8.52$ ppm, **1Z**: $\delta=8.50$ ppm) and OH protons (**1E**: $\delta=12.04$ ppm, **1Z**: $\delta=12.55$ ppm) in $CDCl_3$. The large downfield shift of the OH proton also supports strong intramolecular hydrogen bonding for both **1E** and **1Z**.

The UV/Vis absorption spectra of both isomers were acquired in CH_2Cl_2 and are depicted in Figure 3. Evidently, despite the similarity in the lowest lying transition (S_0–S_1) in the region of 580 nm, salient differences are observed around 350–500 nm, in which **1Z** exhibits additional high-lying absorption bands at about 462 and about 383 nm (see also the closely matched excitation spectra in the Supporting Information, Figure S2), while these bands are rather small in **1E**. Moreover, despite slight changes of the S_0–S_1 absorption feature in various solvents (see Figure S3, Supporting Information), as depicted in Figure 4, remarkable emission solvatochromism was observed for both **1Z** and **1E**. For example, the emission peak wavelength for **1Z** (**1E**) is greatly shifted from 615 nm (612 nm) in cyclohexane to 702 nm (690 nm) in CH_2Cl_2, and this indicates large changes in dipole moment in the excited state. The results verify the original concept of efficient ICT based on the D–A–D pattern in both isomers (vide supra). Many salen Schiff bases with intramolecular hydrogen bonds undergo excited-state intramolecular proton transfer (ESIPT).[10] However, ESIPT was not observed in either **1Z** or **1E**, plausibly due to the dominant intramolecular charge-transfer (ICT) effect, such that solvent dipole relaxation greatly stabilizes **1Z*** (or **1E***) in the equilibrium polarization and hence prevents ESIPT. Several relevant cases have been reported recently.[11]

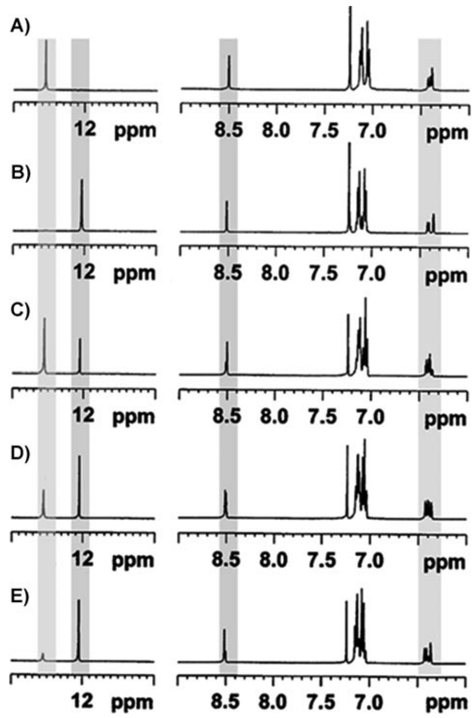

Figure 2. ^{1}H NMR spectrum of A) **1Z** and B) **1E** in $CDCl_3$. ^{1}H NMR spectra of **1Z** after irradiation (GaN laser, 406 nm, 5 mW cm^{-2}) for C) 15, D) 45, and E) 100 min.

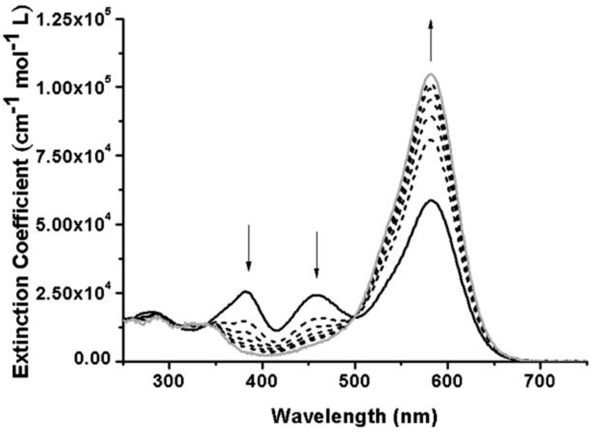

Figure 3. Absorption spectra of **1Z** (black solid line) and **1E** (gray solid line) in CH_2Cl_2. Irradiation (GaN laser, 406 nm) of **1Z** (dashed line) in CH_2Cl_2 as a function of the exposure time at increments of 5 min.

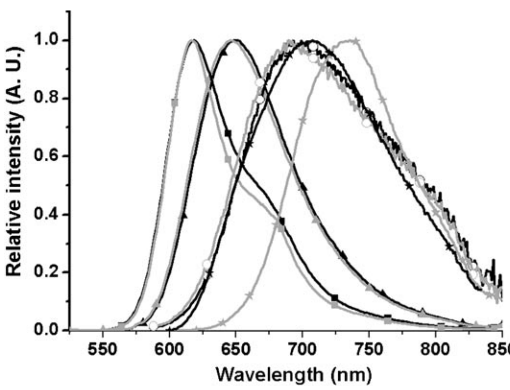

Figure 4. Normalized emission spectra of **1Z** (black) and **1E** (gray) in cyclohexane (■), toluene (▲), CH_2Cl_2 (○) and solid crystal (★). λ_{ex} = 530 nm in solution and λ_{ex} = 514 nm in the solid crystal.

Slight spectral differences in emission between **1Z** and **1E** in solution, while not obvious, could still be recognized. The difference in emission, however, becomes much more significant in the solid state. In the emission spectra of single crystals of **1E** and **1Z** (Figure 4), recorded under a confocal microscope, the emission peak of **1E** at about 740 nm is significantly redshifted with respect to that of **1Z** (700 nm). The result may plausibly be rationalized by the difference in molecular packing between **1E** (Figure 1) and **1Z** (see Figure S1 in the Supporting Information). For **1E**, molecules are stacked in parallel along the *b* axis (see Figure 1B), with an estimated perpendicular interplane distance of about 3.5 Å. Most of the slip angles between the transition moments (assumed to be along the molecular axis) of neighboring molecules on the (010) plane of the adjacent layers are smaller than 54.7°, the critical angle for dipole–dipole interactions. These features of the molecular arrangement are reminiscent of a J-aggregate configuration[12] for **1E**. In contrast, similar stacking along the molecular axis no longer exists in the case of **1Z** (see Figure S1 in the Supporting Information), consistent with a salient difference in emission and morphology between **1Z** and **1E** crystals. Note that the emission position of the solid crystal does not correspond to those in cyclohexane or dichloromethane. This can be rationalized by crystal packing effects such as π–π stacking and dipole–dipole interaction, which commonly alter emission spectral properties significantly.

1Z→1E photoisomerization: Since the difference in experimental conditions to obtain **1E** and **1Z** lies in the presence and absence of room light, it is reasonable to propose that the originally prepared isomer **1Z** is converted to **1E** by photoexcitation during the workup procedure in solution, for example, purification and recrystallization. To verify this hypothesis, Figure 3 depicts the photoisomerization of **1Z** as a function of exposure time on 406 nm excitation. Note that **1E** has a negligible absorption coefficient at 406 nm in CH_2Cl_2, so that interference from product (**1E**) excitation can be avoided. During exposure to the excitation light (406 nm), depletion of the **1Z** form was clearly observed, as indicated by the decrease in the 462 and 383 nm bands, accompanied by an increase of the 582 nm peak, presumably due to production of **1E**. The existence of only **1Z** and **1E** isomers in solution is supported by the observation of an isosbestic point at about 500 nm throughout photoisomerization (see Figure 3). At the end of photoisomerization, as indicated by the disappearance of the 383 and 462 nm bands, the absorption spectrum of the product is identical to that of **1E**, confirming photoinduced **1Z→1E** photoisomerization. Further support was provided by the ^{1}H NMR spectra of **1Z** (see Figure 2C–E), in which the imine and OH proton peaks at $\delta = 8.50$ and 12.55 ppm, respectively, decreased under the excitation light, accompanied by an increase of the proton peaks at $\delta = 8.52$ and 12.04 ppm, characteristic of imine and OH protons, respectively, of the **1E** isomer (cf. Figure 2A and B). Conversely, 605 nm excitation (10 mW cm^{-2}) of pure **1E** for a period of, for example, 2 h, leads to negligible **1E→1Z** photoisomerization, as supported by the lack of any spectral changes in both UV/Vis and ^{1}H NMR spectra (not shown). Moreover, thermal interconversion between **1Z** and **1E** was also examined in the dark (298 K, CH_2Cl_2). The results showed negligible isomerization product with either **1Z** or **1E** as the starting material over one week. We attempted to measure the energy barrier between the electronic ground states by heating perdeuteratochlorobenzene solutions of **1E** and **1Z** at 100 °C. Since the NMR spectra of **1E** and **1Z** remained unchanged, we believe that conversion between **1E** and **1Z** does not occur thermally.

Photodynamic measurements revealed fluorescence lifetimes of **1Z** and **1E** of 91 ± 15 and 82 ± 12 ps, respectively, in CH_2Cl_2 (see Table 1), and the rise time of both emissions is system response limited ($\ll$30 ps). The relaxation dynamics were measured by a time-correlated single-photon counting technique. By taking advantage of the low excitation intensity, **1Z→1E** photoisomerization could be avoided during the measurement, as indicated by the negligible change in the absorption spectrum of **1Z** after the time-resolved measurement.

Table 1. Photophysical and photochemical properties of **1Z** and **1E** in various solvents at 298 K.

	1Z					
	λ_{ab}	λ_{em}	Φ_f[a]	τ_f[a]	Φ_{ct}[a] [%]	$10^{-7} k_{ct}$[a]
CH_2Cl_2	383, 462, 582	697	8.3×10^{-3}	91 ± 15 ps	0.23 ± 0.03	2.5 ± 0.3
toluene	382, 460, 578	650	0.48	0.8 ns	1.36 ± 0.03	1.7 ± 0.2
C_6H_{12}	382, 458, 573	619	0.62	3.1 ns	1.87 ± 0.12	0.60 ± 0.05
n-$C_{16}H_{34}$	381, 457, 575	619	0.93	3.4 ns	0.80 ± 0.06	0.24 ± 0.03
	1E					
	λ_{ab}	λ_{em}	Φ_f[a]	τ_f[a]	Φ_{ct}[a] [%]	$10^{-7} k_{ct}$[a]
CH_2Cl_2	583	691	9.0×10^{-3}	82 ± 12 ps	–	–
C_6H_{12}	575	616	0.76	2.1 ns	–	–
n-$C_{16}H_{34}$	575	617	~1.0	2.2 ns	–	–

[a] Φ_f: fluorescence quantum yield, τ_f: fluorescence lifetime, $\lambda_{ex}=450$ nm, Φ_{ct}: yield of *cis–trans* isomerization, k_{ct}: deduced isomerization rate constant in reciprocal seconds.

Clearly, the result from dynamics investigation shows a lack of precursor–successor-type emission between **1Z** and **1E** and hence the possibility of an adiabatic-type isomerization process, that is, along the singlet excited-state potential-energy surface, can be discarded. We then attempted to analyze the product yield in a more quantitative manner. In a photoinduced isomerization experiment using a 26 mW/cm^2, 406 nm GaN laser to illuminate the entire volume of **1Z** solution (2.1×10^{-5} M in CH_2Cl_2) with a set of lenses with vigorous stirring for, for example, 5 min, we observed that the absorbance at 406 nm decreased from 0.29 to 0.18, corresponding to an increase of 7.9×10^{-6} M in **1E** production. Because of the small absorbance (<0.3 at 406 nm) applied in this experiment, irradiation was considered to be homogenous and any inner-filter effect could be neglected. By taking the ratio for the number of **1E** molecules being produced to the number of photons being absorbed, the product yield Φ_{ct} can be deduced [Eq. (1)],[13]

$$\Phi_{ct} = \frac{V\Delta A_{406}/\varepsilon b}{[P_0 - P(t)]\Delta t/h\nu} \quad (1)$$

where V is the irradiated volume, ΔA_{406} the change in absorbance at 406 nm, ε the extinction coefficient (406 nm), b the cell length, P_0 the transmitted laser intensity when pure CH_2Cl_2 solution was used as reference, and P the transmitted intensity, recorded every 5 s (Δt) during irradiation of the samples. Thus, the yield of **1E** production was determined to be (0.23 ± 0.03)%. The relatively low yield of **1E** production, together with a lack of correlation between **1E** and **1Z** in emission dynamics, leads us to conclude that the isomerization reaction takes place nonadiabatically, perhaps from the S_1 (**1Z**) to S_0 (**1E**) potential-energy surface.[14a–f] Further support of this hypothesis is given by the similar observation of **1Z***→**1E** isomerization in nonpolar solvents such as toluene, cyclohexane, and n-hexadecane. According to time-correlated single-photon measurements, the fluorescence lifetimes of **1Z** and **1E** (see Table 1) are as long as 0.8, (3.1, 3.4) and (2.1, 2.2) ns, respectively, in toluene, (cyclohexane, n-hexadecane), while photoinduced (406 nm) **1Z**→**1E** isomerization still takes place (see Figures S4 and S5 in the Supporting Information). By using the same method as in CH_2Cl_2, the yields of **1E** production in toluene, cyclohexane, and n-hexadecane were then calculated to be (1.36 ± 0.03), (1.87 ± 0.12), and (0.80 ± 0.06)%, respectively.

On excitation, followed by the ultrafast ($\leqslant$10 ps) internal conversion and solvent and vibrational relaxation, the decay dynamics of the S_1 state in **1Z** can be expressed as Equation (2),

$$\frac{d[S_1]}{dt} = -k_r[S_1] - k_{nr}[S_1] - k_{isc}[S_1] - k_{ct}[S_1] = -k_{obs}[S_1] \quad (2)$$

where k_r and k_{nr} are the radiative and nonradiative decay (except for *cis–trans* isomerization) rate constants, k_{isc} is the rate constant of $S_1 \rightarrow T_1$ (or T_n, $n>1$) intersystem crossing, k_{ct} the *cis–trans* isomerization rate constant, and k_{obs} the experimentally observed decay rate. Since the yield of photoisomerization is independent of the presence of O_2, that is, similar results were obtained for aerated and degassed solutions, the possibility that photoisomerization mainly takes place in the triplet manifold can be discarded. Accordingly, the yield of **1E** production Φ_{ct} can be expressed as Equation (3).

$$\Phi_{ct} = \frac{k_{ct}}{k_r + k_{nr} + k_{isc} + k_{ct}} = \frac{k_{ct}}{k_{obs}} \quad (3)$$

For example, in CH_2Cl_2, k_{obs} was measured to be 1.1×10^{10} s^{-1} ($\tau_f=91$ ps). Taking Φ_{ct} of (0.23 ± 0.03)%, the *Z–E* isomerization rate was then deduced to be $(2.5\pm0.3)\times10^7$ s^{-1}. The radiative decay rate k_r of the S_1 state for **1Z** can thus be calculated from the fluorescence yield Φ_f expressed as Equation (4),

$$\Phi_f = k_r/k_{obs} \quad (4)$$

where Φ_f was measured to be 8.3×10^{-3} for **1Z** in CH_2Cl_2. Accordingly, k_r was deduced to be 9.12×10^7 s^{-1} in CH_2Cl_2 (see Table 1). In theory, k_{isc} should be small in **1Z** due to the forbidden $S_1(\pi\pi^*) \rightarrow T_1(\pi\pi^*)$ intersystem crossing invoking weak vibronic coupling and negligible heavy-atom effect. This means that k_{nr} is the dominant part for S_1 relaxation in CH_2Cl_2. This is expectable, since **1Z** (or **1E**) in the excited state has pronounced charge-transfer character and hence is subject to solvent-polarity quenching. The quenching effect was apparently small (vide supra) in cyclohexane and n-hexadecane owing to less solvent relaxation. The consequence of larger emission gap is reflected in the relatively large fluorescence yields Φ_f of 0.48, 0.62, and 0.93 for **1Z** in toluene, cyclohexane, and *n*-hexadecane, respectively (see Table 1). Similarly, with the known Φ_{ct} and k_{obs} values (see Table 1), the *cis*/*trans* isomerization rate constant k_{ct} was then deduced to be $(1.7\pm0.2)\times10^7\,s^{-1}$, $(6.0\pm0.5)\times10^6\,s^{-1}$, and $(2.4\pm0.3)\times10^6\,s^{-1}$ in toluene, cyclohexane, and *n*-hexadecane, respectively.

Figure 5 shows a plot of the photoinduced **1Z***→**1E** isomerization rate constant versus the reciprocal of solvent viscosity η. Within experimental error, the linear plot indicates

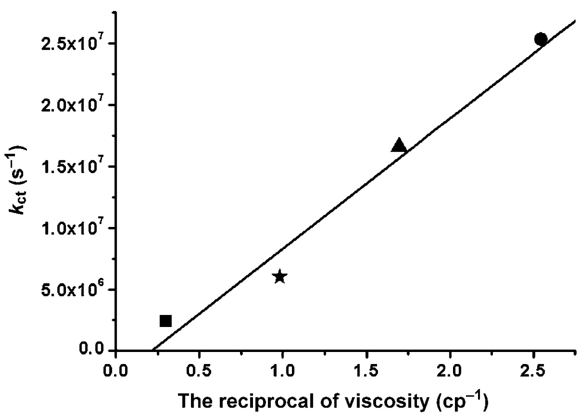

Figure 5. Plot of the **1Z**→**1E** isomerization rate constant k_{ct} versus the reciprocal of solvent viscosity in CH_2Cl_2(●), toluene(▲), cyclohexane (★), and *n*-hexadecane(■). $R^2=0.97$.

that the **1Z**→**1E** isomerization rate constant is inversely proportional to the viscosity of the solvent. Since the photoinduced **1Z** (*cis*)→**1E** (*trans*) isomerization mainly involves a large amplitude motion of either wing (see Scheme 1), such a motion is strongly coupled to the medium, with high friction. In this case, the velocity relaxation time τ_c should be considerably shorter than the characteristic timescales of free motion on the potential surface. Accordingly, in the Smoluchowski limit,[15] the rate constant becomes inversely proportional to the frictional coefficient ζ and hence to the viscosity η, assuming a hydrodynamic model in which $\zeta\propto\eta$. Nevertheless, recent studies by Tahara and co-workers[14g] on *cis–trans* photoisomerization of stilbene suggested that the reaction is a two-step process, initiated by elongation of the double bond, followed by out-of plane twisting motion of the vinylic hydrogen atom. The dipolar changes lead to the solvent-polarity effect on the rate of isomerization. In the present case of **1Z**→**1E** isomerization, due to the changes in dipole moment, solvent polarity may also induce a non-negligible barrier that channels into the reaction.

To gain more insight into the above photophysical and photochemical behavior, calculations were performed on the thermodynamics and electronic transition properties of **1Z** and **1E**. By geometrical optimization of their structures at the TD-B3LYP/6-31G** level of density functional theory,[16] together with modeling of solvation (e.g., CH_2Cl_2) by using the integral equation formalism polarizable continuum (IEFPCM) model,[17] **1Z** was calculated to be 7.70 kcal mol^{-1} higher in energy than **1E**. This result is expected due to the significant steric interaction between the two 4-(di-*p*-tolylamino)-2-hydroxybenzylideneamino wings in **1Z**. By using the TD-B3LYP method, the vertical (i.e., Franck–Condon) excitation energy from the ground state to the lowest lying excited state in the singlet manifold was also calculated. Table 2 depicts the features of the LUMOs and HOMOs that are mainly involved in the S_1 transition for **1Z** and **1E**. The descriptions, energy gaps, and oscillator strengths of the lowest lying singlet transitions are also listed in Table 2. The calculated S_1 energy levels of **1Z** (545 nm) and **1E** (537 nm) are close and are qualitatively consistent with those obtained from the absorption (S_1) spectra. Evidently, for both **1Z** and **1E**, substantial electron density at the amino sites in the HOMO shifts to cyano sites in the LUMO, in firm support of charge transfer on electronic excitation. When solvation effects (CH_2Cl_2) are taken into account by means of the IEFPCM model, the $S_0\rightarrow S_1$ transitions of **1Z** and **1E** in CH_2Cl_2 bathochromically shift from 545 nm (gas) to 603 nm (CH_2Cl_2) and 537 nm (gas) to 597 nm (CH_2Cl_2) respectively. The apparent redshift further confirms the ICT behavior. As shown in Table 2, for both **1Z** and **1E** conformers, S_2 and S_3 are mainly associated with HOMO−1→LUMO and HOMO−2→LUMO, respectively, in which HOMO−1 and HOMO−2 are ascribed to lone pairs of nitrogen atoms on the amino groups and π orbitals plus lone pairs of oxygen atoms on the phenol fragments. Notably, the associated oscillator strengths (S_2: 0.27 and S_3: 0.09) for **1Z** are significantly larger than those of **1E** (S_2: 0.01, S_3: 0.04; see Table 2), which are qualitatively consistent with the salient differences in absorptivity for the higher lying absorption bands between **1Z** and **1E** (see region of 300–500 nm in Figure 3). This may be due to the symmetry restriction, in which the Z (*cis*) form imposed by C_{2v} symmetry is less constrained in electronic transition than the *E* (*trans*) form with C_{2h} symmetry.

To construct the photoinduced isomerization pathways in a qualitative manner, we simply add the observed $S_0\rightarrow S_1$ absorption peak frequency for the respective **1Z** and **1E** to the relative ground state thermodynamics calculated for **1Z** and **1E**. The results are depicted in Scheme 2. As indicated by a ΔH value of $-7.7\,kcal\,mol^{-1}$, the **1Z**→**1E** isomerization is exergonic (assuming similar entropic factor) in both the ground and first excited states (in the singlet manifold). However, despite its thermally favorable nature, experimental results indicate that **1Z**→**1E** isomerization is kinetically unfavorable in the ground state, most plausibly due to a high barrier on twisting about the strong C2−C2A double bond (Figure 1 A). In the electronically excited state, as supported by the frontier orbital analysis (Table 2), the C2−C3 (C2−C2A) bonding in the LUMO for **1Z** (**1E**) has substantial antibonding character due to the charge-transfer reaction. Accordingly, facile rotation around the maleonitrile C=C bond is expected, inducing **1Z**→**1E** isomerization, as evidenced by production of **1E**. Nevertheless, the experimental results also indicate that the **1Z***→**1E** channel only accounts for minor fraction among overall relaxation processes (vide supra) and hence attempts to resolve the barrier associated

Table 2. Descriptions, energy gaps, and oscillation strengths of the first three singlet transitions and the associated frontier orbitals for **1Z** and **1E**.

1Z

	Excitation	E_{cal} [eV]	λ_{cal}	f
S_1	HOMO→LUMO (+84%)[a]	2.27	545.4	0.95
	HOMO→LUMO (+87%)[b]	2.05	603.4	0.98
S_2	HOMO−1→LUMO (+87%)[a] HOMO→LUMO+1 (6%)[a]	2.70	459.9	0.27
S_3	HOMO−2→LUMO (+82%)a	3.15	393.5	0.09

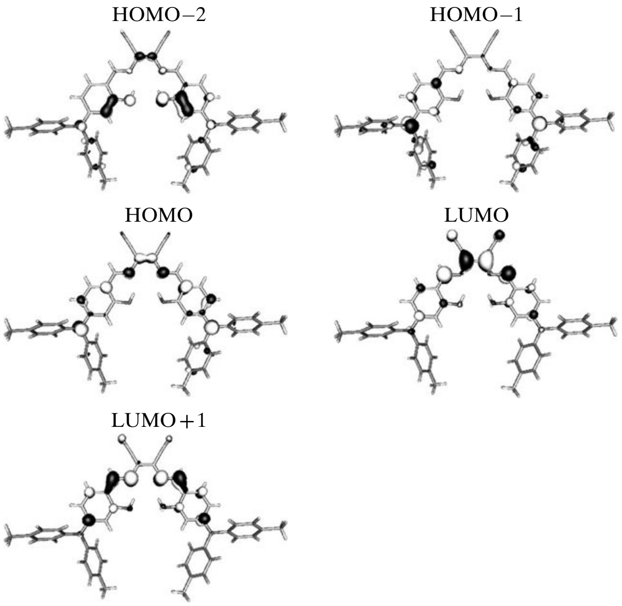

1E

	Excitation	E_{cal} [eV]	λ_{cal}	f
S_1	HOMO→LUMO (+81%)[a]	2.31	537.1	1.0
	HOMO→LUMO (+85%)[b]	2.08	596.7	1.0
S_2	HOMO−1→LUMO (+88%)[a] HOMO→LUMO+1 (+5%)[a]	2.75	451.0	0.01
S_3	HOMO−2→LUMO (+83%)[a]	3.19	389.2	0.04

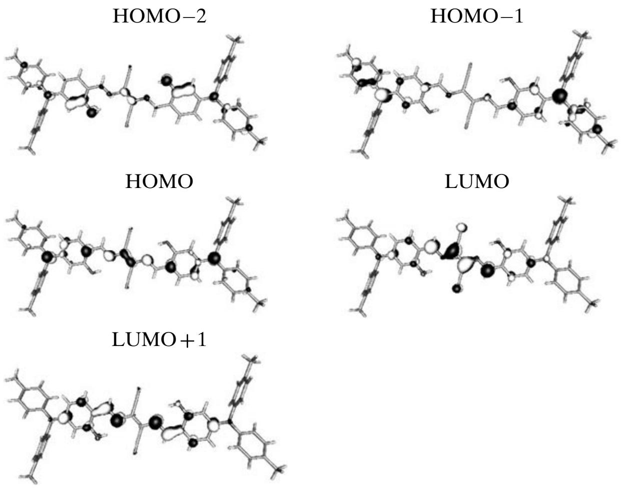

[a] In the gas phase. [b] Data obtained in CH_2Cl_2 by IEFPCM.

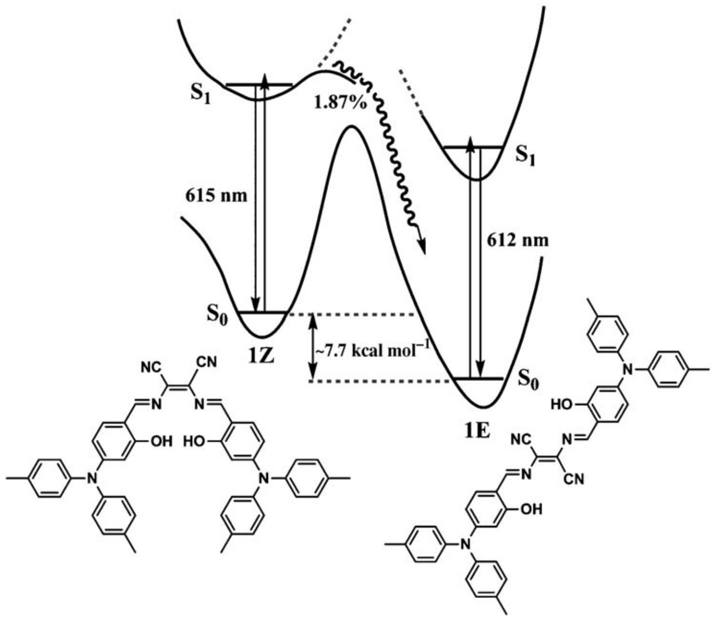

Scheme 2. Proposed **1Z**→**1E** photoisomerization and relative thermodynamics in cyclohexane. The potential-energy surfaces are depicted in a qualitative manner.

with isomerization are not further pursued. Nonetheless, strong correlation between rate of **1Z***→**1E** isomerization and solvent viscosity is evident. The result thus cannot exclude **1Z***→**1E** isomerization being limited by the viscosity barrier.

Coordination chemistry of *E*/*Z* isomers: From the viewpoint of coordination chemistry, the reaction of **1E** and **1Z** with transition metals forming the corresponding complexes should be of great interest. Hence, we attempted to synthesize Zn^{II} complexes of **1Z** and **1E** as ligands. In one approach, reaction of $Zn(OAc)_2$ with **1Z** in the dark yielded a deep-red product, denoted as Zn^{II}/**1Z**, crystals of which were successfully grown and characterized by X-ray analysis (Figure 6).

In Zn^{II}/**1Z** the **1Z** dianion serves as a tetradentate chelating ligand, and a water molecule added to the fifth vertex to form a pyramidal structure. Two 4-(di-*p*-tolylamino)-2-(iminomethyl)phenol moieties are virtually in a *cis* configuration relative to the maleonitrile C=C bond. The main molecular skeleton is in a slightly twisted configuration, as indicated by the nonsymmetric structure around the metal center, plausibly due to the electrophilic property of the metal atom as well as the fact its size is larger than the void site provided by the tetradentate ligand. Five-coordinate salen metal complexes are more stable than four-coordinate ones,[18,19] and Zn^{II} and the **1Z** ligand are not coplanar due to coordination of a water molecule. Nevertheless, the salicylimine moiety remains planar mainly because of its coordination to the core Zn^{II} atom. Both UV/Vis absorption and emission spectra of the Zn^{II}/**1Z** complex (see Figure S6 in Supporting Information) are similar to that of **1Z** (cf. Figure 3 for **1Z**), except that the full width at half-maximum (ca. 2265 cm^{-1})

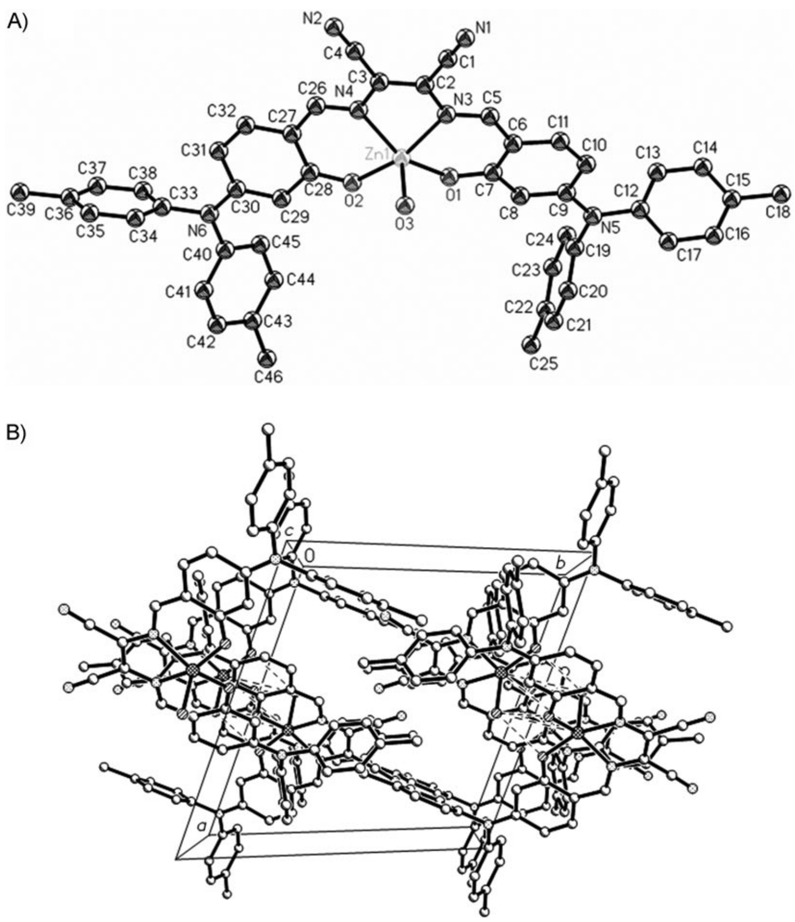

Figure 6. A) Structure of Zn^{II}/**1Z** with thermal ellipsoids set at 30% probability. Selected bond lengths [Å]: Zn1−O1 1.9772(15), Zn1−O2 1.9780(16), Zn1−O3 2.0558(19), Zn1−N3 2.0875(19), Zn1−N4 2.0725(19), N3−C2 1.375(3), N3−C5 1.3143), N5−C9 1.370(3), N5−C12 1.444(3), N3−C19 1.446(3), N4−C3 1.383(3), N(4)−C26 1.312(3), N6−C30 1.375(3), N6−C33 1.445(3), N6−C40 1.436(3), C2−C3 1.373(3), C5−C6 1.409(3), C26−C27 1.404(3). Detailed data are summarized in the Supporting Information. B) Molecular arrangement of Zn^{II}/**1Z** viewed along the *c* axis.

for the emission of Zn^{II}/**1Z** is smaller than that of **1Z** (ca. 2780 cm^{-1} in CH_2Cl_2). This may be rationalized by incorporation of the Zn^{II} ion in the Zn^{II}/**1Z** complex, which enhances the rigidity of the molecular framework. Efforts were also made to explore the coordination chemistry of **1E**. However, as evidenced by lack of changes in ^{1}H NMR, UV/Vis, and fluorescence spectra, **1E** failed to react with $Zn(OAc)_2$ to produce any corresponding Zn^{II}/**1E** complexes that could be characterized spectroscopically. The lack of a tetradentate site for square-planar coordination, together with steric hindrance caused by the nitrile group, should account for the low reactivity of **1E** toward Zn^{II} complexation.

To further explore the coordination chemistry between maleonitrile *Z* and *E* forms, we then strategically designed a derivative of **1**, namely, *N*,*N′*-dicyanoethenebis(salicylideneimine)dicarboxylic acid (**2**, see Scheme 1), which shares the same core moiety as **1**, but has additional carboxyl functional groups in the *para* positions to the hydroxyl groups. The aim of this approach is twofold: 1) To unify the photoinduced *E*/*Z* isomerization for maleonitrile-type salen Schiff bases. 2) To expand the scope by investigating the differences of *E*/*Z* isomers in their binding modes toward transition metals. For the latter application, it is noteworthy that infinite coordination polymers (ICPs) have aroused enormous attention. Hybrid materials have been built from metal ions and polydentate bridging ligands, of which salen-type ligands are among the most common building blocks.[20,21] Because of their appropriate coordinating functionalities (COOH), we propose that **2Z** (**2E**) with its intrinsic structure-building motif would be a suitable template to demonstrate as well as to differentiate maleonitrile *E*/*Z* conformers leading to different coordination polymers with transition metal ions as nodes. As depicted in Scheme 1, a condensation process[8,9] involving *cis*-diaminomaleonitrile and 3-formyl-4-hydroxybenzoic acid[22] in methanol afforded **2Z** by *syn* addition, as evidenced by the ^{1}H NMR spectrum (Figure 7A, see Experimental Section for further characterization). Compound **2Z** exhibits an $S_0 \rightarrow S_1$ absorption maximum at 490 nm in dimethyl sulfoxide (DMSO). On 490 nm excitation, monitoring the changes in ^{1}H NMR spectra showed that **2Z** also undergoes photoisomerization to **2E**. ^{1}H NMR spectroscopic studies revealed that the corresponding peaks of **2E** were generated, and the chemical shifts of protons associated with the reaction had changed. In particular, the resonances for imine protons H_a and H_b (see Figure 7B) are shifted upfield from $\delta = 8.61$ and 8.56 ppm (**2Z**) to $\delta = 8.50$ and 8.31 ppm (**2E**).

Nevertheless, unlike the photoinduced **1Z**→**1E** process with unity yield, the photoisomerization reaches a state of saturation in which the ratio of **2Z** to **2E**, calculated by NMR integrals, is determined to be about 2:1. (Figure 7B) This ratio remains unchanged after ceasing photoexcitation. The results indicate involvement of a dual pathway, that is, **2Z***→**2E** and **2E***→**2Z**, amid photoinduced isomerization, as occurs in many photoinduced *cis*–*trans* isomerizations.[23] Fortunately, since **2E** is less soluble than **2Z** in DMSO, it could be isolated by repeated recrystallization from DMSO in the dark (see Experimental Section). Note that in this study **2Z** and **2E** were mainly applied as a prototype to in-

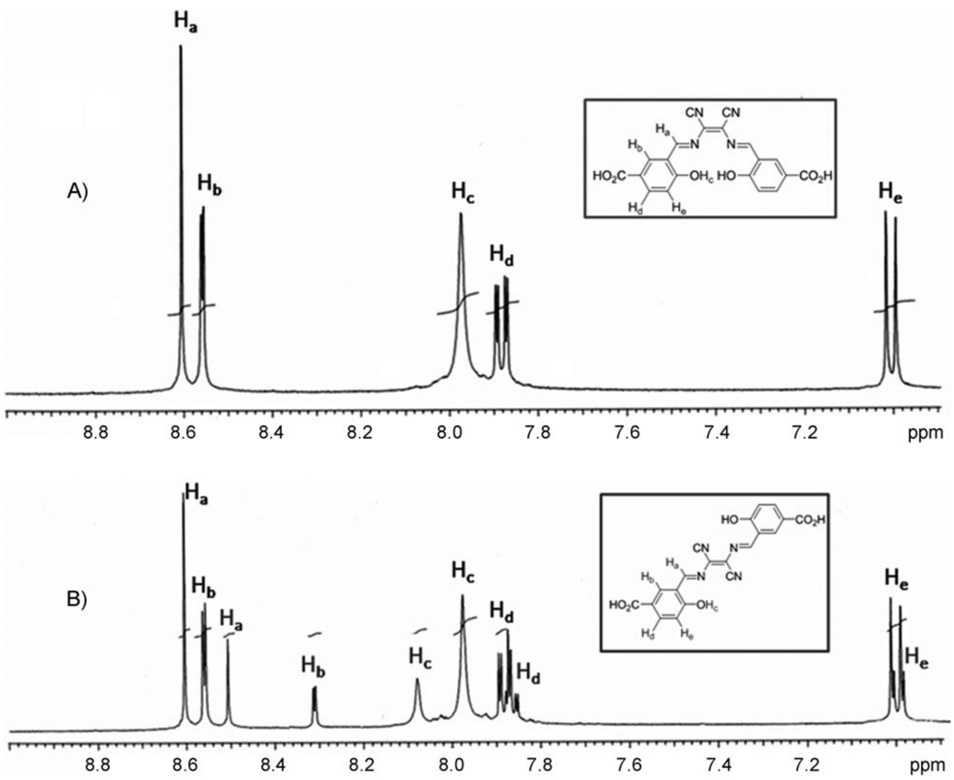

Figure 7. A) ^{1}H NMR spectra of pure **2Z**. B) After exposure to room light for 1 day, peaks of **2E** are generated, and the ratio of **2Z**/**2E** is 2/1.

vestigate the difference in ICP, and thus detailed photoisomerization dynamics were not further pursued.

To study the difference in morphology between Zn^{II}/**2Z** and Zn^{II}/**2E**, we first chose pure **2Z** as a precursor to synthesize ICPs (Figure 8A and B). Since **2Z** would undergo photoinduced isomerization, all glassware was wrapped in aluminum foil to exclude light. After reaction of **2Z** with zinc acetate, Zn^{II}/**2Z** was collected from the reaction mixture by centrifugation and washed with methanol to remove any unconsumed $Zn(OAc)_2$. The resulting particles were found to be stable in organic solvents (hexane, dichloromethane, methanol, acetone, DMSO) and as a dried solid. The chemical composition of Zn^{II}/**2Z** was determined by energy-dispersive X-ray spectroscopy (Figure 8D), the results of which clearly revealed that zinc ions had coordinated with **2Z**. Further elemental analysis (see Experimental Section) confirmed the formation of a 1:2 structure derived from a deprotonated ligand **2Z**-4H and $2Zn^{II}$ per repeat unit. Coordination between metal ions and carboxylate-functionalized ligands is well-known in transition metal coordination chemistry, and it can be characterized by IR spectroscopy.[20,21,24] On coordinating with Zn^{II}, deprotonation of the carboxyl group results in a decrease in C=O stretching frequency from $1672\,cm^{-1}$ for the precursor (**2Z**) to $1618\,cm^{-1}$ for the polymer particles (see Experimental Section). Figure 8B shows the morphology of the as-prepared ICPs, as characterized by field-emission scanning electron microscopy (FESEM); the image shows spherical particles with an average size of 85 ± 15 nm. The spherical morphology of Zn^{II}/**2Z** ICPs is similar to that of Zn^{II}/salen acid ICPs reported by Oh and Mirkin;[20] the first equivalent of Zn^{2+} coordinates to the salen pocket, and the other equivalent acts as a linker that connects two carboxylate groups with formation of coordination polymers.

We then used **2E** and $Zn(OAc)_2$ to prepare ICPs by a similar procedure under dim red light to avoid photoisomerization. As shown in Figure 8C, FE-SEM revealed an exclusively linear, needlelike morphology. Elemental analyses (see Experimental Section), and the energy-dispersive X-ray spectrum (Figure 8E) are consistent with formation of a 1:1 structure derived from Zn^{II} and a deprotonated ligand **2E**-2H per repeat unit. The shift of C=O stretching frequency from $1670\,cm^{-1}$ for the precursor (**2E**) to $1{,}615\,cm^{-1}$ for Zn^{II}/**2E** ICPs indicates coordination of Zn^{II} and the carboxylate moiety. Similar to **1E**, it is reasonable to conclude that the salen bidentate site is not involved in Zn^{II} coordination due to the steric hindrance introduced by the nitrile group, while bidentate binding of carboxylate groups from two **2E**-2H ligands to Zn^{II} leads to formation of linear ICPs (Figure 8C).

With the *E* conformation of **2E**, the shape of Zn^{II}/**2E** ICPs can be rationalized by linear, *trans*-oriented Zn^{II}/carboxylate coordination, which is in sharp contrast to spherical Zn^{II}/**2Z** ICPs resulting from alternative Zn^{II}/carboxylate and Zn^{II}/salen coordination. In addition to the difference in shape, Zn^{II}/**2E** ICPs have a longitudinal length of 2 ± 0.5 μm, which is much larger than Zn^{II}/**2Z** ICPs with a diameter of 85 ± 15 nm. Such an ultimate size may reflect the number of seeds involved in the aggregation process, and is likely affected by the solubility of the precursor.[25] The lower solubility of **2E** (vs. **2Z**) in, for example, DMSO leads to a greater tendency for aggregation, which results in larger metal-organic frameworks.

We also recorded absorption and emission spectra for **2Z**, **2E** and their Zn^{II} ICPs. The results shown in Figure 9 indicate that the fluorescence of both ICPs is redshifted from those of their parent **2Z** and **2E** precursors. Moreover, despite negligible difference in absorption and emission peak between **2Z** and **2E** in solution (e.g., DMSO), notable changes are observed for Zn^{II}/**2Z** versus Zn^{II}/**2E** ICPs, in that the emission peak of about 690 nm in Zn^{II}/**2Z** is red-

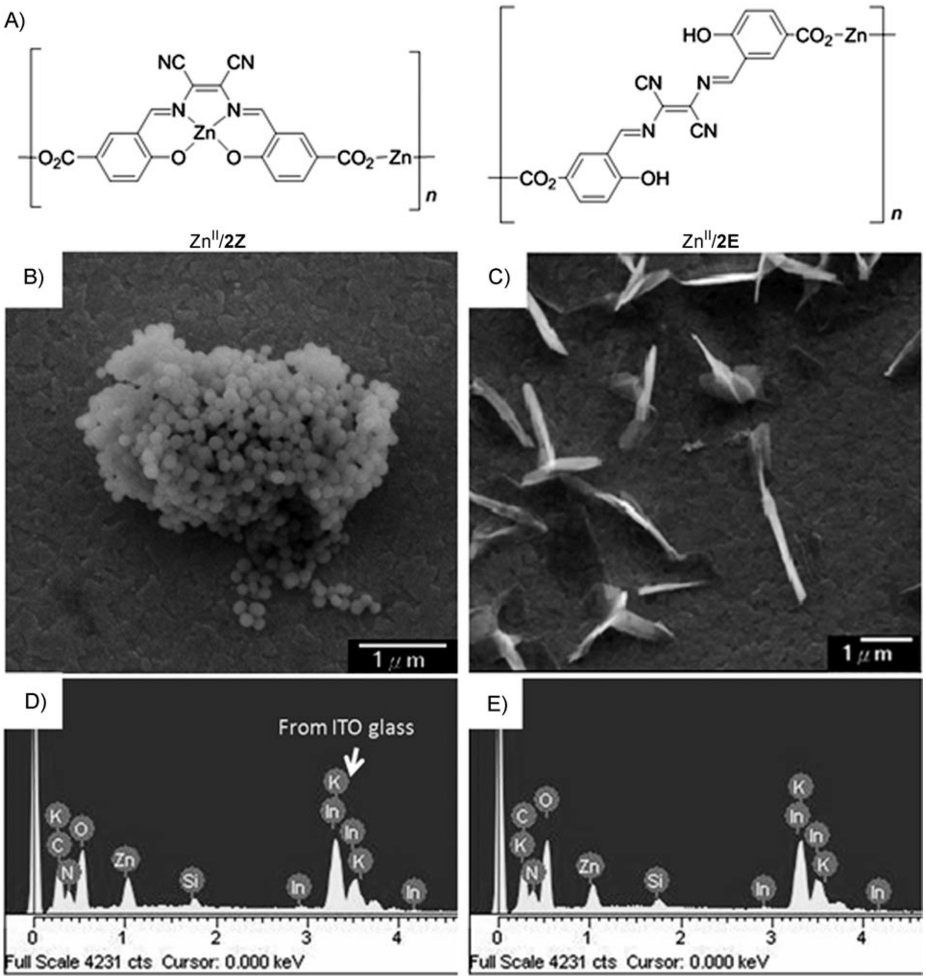

Figure 8. A) Proposed ICP structures for Zn^{II}/**2Z** and Zn^{II}/**2E.** B) SEM image of Zn^{II}/**2Z**; the shape is spherical, and the size is about 85 ± 15 nm. C) SEM image of a mixture of Zn^{II}/**2Z** and Zn^{II}/**2E**; since Zn^{II}/**2Z** is spherical, the thin strips are assigned as Zn^{II}/**2E**. D) EDX spectrum of Zn^{II}/**2Z**. E) EDX spectrum of Zn^{II}/**2E**.

shifted by about 30 nm with respect to that in Zn^{II}/**2E** ICPs (ca. 660 nm). The results can be rationalized by the additional tetradentate coordination in the salen pocket of Zn^{II}/**2Z** ICPs, which elongates the π conjugation. Accordingly, prominent differences between *Z*- and *E*-type salen coordination chemistry are established.

Conclusions

We have explored facile photoinduced $Z\rightarrow E$ isomerization of salen ligand **1**. Both **1Z** and **1E** isomers are thermally stable in the absence of light. Firm support has been given by X-ray structural analysis, ^{1}H NMR spectroscopy, and the associated photophysical properties. The **1Z**→**1E** isomerization is triggered by rotation about the C2–C3 bond (**1Z**), which takes on single-bond character due to photoinduced charge transfer. The isomerization reaction plausibly takes place nonadiabatically from the excited-state (**1Z**) to the ground-state (**1E**) potential-energy surface in the singlet manifold. The inverse proportionality between isomerization rate constant and solvent viscosity indicates a large-amplitude motion that is strongly coupled with the solvent medium during the reaction. Although photoinduced isomerization has been reported in numerous Schiff bases,[26] to the best of our knowledge, no examples have been demonstrated in salen ligands involving four coordination sites. This finding led to further exploration of the differences in coordination chemistry between **1Z** and **1E** with respect to forming Zn^{II} complexes. To further explore the difference in coordination chemistry, we then synthesized **2Z** and **2E** and their corresponding Zn^{II} ICPs, for which we found distinct differences in morphology. Interestingly, most metal complexes coordinated by **1Z**-analogous salen-type ligands, that is, with D–A–D arrangement, have been reported to have the *Z* configuration.[8,9] Thus, our finding of photoinduced $Z\rightarrow E$ isomerization of a *Z*-configured maleonitrile salen Schiff base may pave a new avenue in chemistry. For example, on metal coordination, the two forms might show different catalytic activities for asymmetric reactions.[27] We thus believe that the results pre-

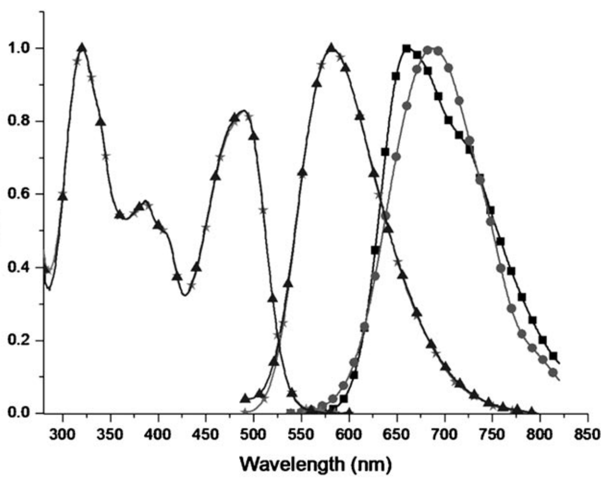

Figure 9. Emission spectra of **2Z** (★), **2E** (▲), pure Zn^{II}/**2Z** (●), and mixture of Zn^{II}/**2Z** and Zn^{II}/**2E** (■).

sented in this study should spark a broad spectrum of interest in research on salen ligands.

Experimental Section

General information and materials: All operations were carried out by using standard Schlenk techniques under nitrogen atmosphere. NMR spectra were recorded at room temperature on Bruker and Varian spectrometers operating at 300, 400, and 500 MHz (^{1}H NMR) and 125 MHz (^{13}C NMR), and chemical shifts δ are reported in ppm with residual protons in the solvent as standard ($CDCl_3$: $\delta = 7.24$, [D$_8$]THF: $\delta = 1.74$, [D$_6$]DMSO: $\delta = 2.50$). 2-Hydroxy-4-(di-*p*-tolylamino)benzaldehyde was obtained by a modification of the previously reported procedure.[7] All other reagents were used as received from commercial suppliers. Elemental analysis was performed on a Perkin-Elmer 2400 CHN at the NSC Regional Instrumentation Center at National Taiwan University, Taipei, Taiwan. Fast atom bombardment mass spectra (FAB-MS) were recorded on a JEOL SX-102 A.

Synthesis of 2,3-bis[4-(di-*p*-tolylamino)-2-hydroxybenzylideneamino]maleonitrile (1): Compound **1** was prepared according to the method reported by Lacroix and co-workers[8] with slight modification. In brief, a mixture containing diaminomaleonitrile (108 mg, 1.0 mmol) and 2-hydroxy-4-(di-*p*-tolylamino)benzaldehyde (635 mg, 2.0 mmol) was stirred overnight at room temperature in 20 mL of absolute ethanol containing one drop of sulfuric acid as catalyst. The dark red precipitate was then collected by filtration and washed with ethanol (657 mg, 93 % yield). All synthesis and workup procedures were performed under dim light with $\lambda > 700$ nm. On recrystallization from toluene in the dark, green needle-shaped crystals of **1Z** were obtained. Then, under fluorescent light, the **1Z** isomer was re-dissolved in benzene and further recrytallized by slow diffusion of ethanol into the benzene solution for several days. The resulting dark green crystals, according to X-ray analysis, were assigned to the **1E** isomer. Elemental analysis calcd (%) for $C_{46}H_{38}N_6O_2$: C 78.16, H 5.42, N, 11.89; found for **1Z**, **1E**: C 78.13, 78.10, H 5.49, 5.50, N 11.70, 11.68. **1Z**: ^{1}H NMR (500 MHz, $CDCl_3$): $\delta = 2.33$ (s, 12H, CH_3), 6.39 (d, 2H, Ph, $^4J_{H,H} = 2.0$ Hz), 6.42 (dd, 2H, Ph, $^3J_{H,H} = 8.5$ Hz, $^4J_{H,H} = 2.0$ Hz), 7.04–7.13 (m, 18H, Ph), 8.50 (s, 2H, N=CH), 12.55 ppm (s, 2H, OH); ^{13}C NMR (125 MHz, $CDCl_3$): $\delta = 21.0$, 104.4, 111.0, 111.9, 112.2, 122.7, 127.0, 130.4, 134.8, 136.0, 142.6, 155.4, 162.9 (N=CH), 163.9 ppm. **1E**: ^{1}H NMR (500 MHz, $CDCl_3$): $\delta = 2.33$ (s, 12H, CH_3), 6.36 (d, 2H, Ph, $^4J_{H,H} = 1.7$ Hz), 6.41 (d, 2H, Ph, $^3J_{H,H} = 8.9$ Hz), 7.06–7.16 (m, 18H, Ph), 8.52 (s, 2H, N=CH), 12.04 ppm (s, 2H, OH); ^{13}C NMR (125 MHz, $CDCl_3$): $\delta = 21.0$, 104.5, 110.9, 111.2, 111.8, 125.3, 126.9, 130.4, 134.6, 135.9, 142.7, 155.1, 162.4 (N=CH), 163.4 ppm: FAB-MS: m/z 706.8, 706.7 [M^+] (**1Z**, **1E**).

Synthesis of the Zn^{II}/1Z Zn^{II}/1E complexes: A mixture of 2-hydroxy-4-(di-*p*-tolylamino)benzaldehyde (635 mg, 2.0 mmol), $Zn(OAc)_2{\cdot}2H_2O$ (327 mg, 1.5 mmol) and diaminomaleonitrile (108 mg, 1.0 mmol) was stirred in MeOH/THF (10 mL/20 mL) overnight at room temperature. Then the solvent was removed under vacuum. The residue was washed with methanol and the precipitate collected by filtration. The dark red product was identified as Zn^{II}/**1Z** (493 mg, 64 %). Elemental analysis calcd (%) for Zn^{II}/**1Z** ($C_{46}H_{36}N_6O_2Zn$): C 71.73, H 4.71, N 10.91; found: C 70.10, H 4.49, N 10.70; ^{1}H NMR ([D$_8$]THF): $\delta = 8.27$ (s, 2H, N=CH), 7.15 (d, 4H, Ph, $^3J_{H,H} = 8.2$ Hz), 7.05 (d, 4H, Ph, $^3J_{H,H} = 8.2$ Hz), 7.02 (d, 2H, Ph, $^3J_{H,H} = 9.0$ Hz), 6.14 (dd, 2H, Ph, $^3J_{H,H} = 9.0$ Hz, $^4J_{H,H} = 2.2$ Hz), 6.05 (d, 2H, Ph, $^4J_{H,H} = 2.2$ Hz), 2.33 ppm (s, 12H, CH_3); ^{13}C NMR: $\delta = 174.0$, 156.6, 153.7, 141.6, 134.6, 133.0, 128.0, 125.1, 117.8, 112.6, 109.8, 107.2, 107.1, 18.1 ppm (CH_3); MS (FAB, Zn = 64): m/z 771.2 [$M^+ + 1$]. A mixture of **1E** (100 mg, 0.14 mmol), tetramethylammonium hydroxide (28 mg, 0.3 mmol), and methanol (10 mL) was stirred at room temperature for 30 min. $Zn(OAc)_2{\cdot}2H_2O$ (31 mg, 0.14 mmol) was added to the solution of deprotonated **1E**, which was stirred overnight at room temperature. Some dark purple powder precipitated from the reaction solution. The product was collected by filtration and washed with methanol (1 mL). The detailed identification is summarized in the Supporting Information.

Synthesis of *N,N'*-dicyanoethenebis(salicylideneimine)dicarboxylic acid (2): A mixture of *cis*-diaminomaleonitrile (27 mg, 0.25 mmol) and 3-formyl-4-hydroxybenzoic acid (83 mg, 0.50 mmol) was stirred in methanol (10 mL) for 12 h at room temperature. Then the precipitate was washed with methanol several times and filtered by suction to a pale yellow powder (90 mg, 90 %). IR (KBr pellet): $\tilde{\nu} = 1672$s, 1631s, 1491m, 1453m, 1391w, 1319 m, 1287 m, 932w, 848w, 770w, 674w, 501w, 462w cm^{-1}; elemental analysis calcd (%) for $C_{20}H_{12}N_4O_6$ (**2Z**): C 59.41, H 2.99, N 13.86; found: C 56.67, H 2.78, N 17.31. **2Z**: ^{1}H NMR (400 MHz, [D$_6$]DMSO): $\delta = 7.00$ (d, 2H, Ph, $^3J_{H,H} = 4.4$ Hz), 7.88 (dd, 2H, Ph, $^3J_{H,H} = 4.4$ Hz, $^4J_{H,H} = 2.4$ Hz), 7.97 (s, 2H, OH), 8.56 (d, 2H, $^4J_{H,H} = 2.4$ Hz), 8.61 ppm (s, 2H, N=CH); ^{13}C NMR (100 MHz, [D$_6$]DMSO): $\delta = 114.6$, 118.4, 122.9, 125.8, 130.9, 134.0, 163.7, 169.3 ppm. **2E**: ^{1}H NMR (400 MHz, [D$_6$]DMSO): $\delta = 6.99$ (d, 2H, Ph, $^3J_{H,H} = 4.4$ Hz), 7.86 (dd, 2H, Ph, $^3J_{H,H} = 4.4$ Hz, $^4J_{H,H} = 2.0$ Hz), 8.08 (s, 2H, OH), 8.31 (d, 2H, $^4J_{H,H} = 2.0$ Hz), 8.50 ppm (s, 2H, N=CH); ^{13}C NMR (100 MHz, [D$_6$]DMSO): $\delta = 114.6$, 118.0, 122.9, 125.8, 130.9, 134.0, 163.7, 169.3 ppm.

Synthesis of Zn^{II}/2Z Zn^{II}/2E complexes: A mixture of **2Z** (2.83 mg, 0.007 mmol) and zinc acetate (3.07 mg, 0.014 mmol) was dissolved in DMSO (3 mL). The resulting solution was heated at 80 °C for 1 h. Then the reaction mixture was cooled to room temperature, and the precipitate was collected by centrifugation and washed with methanol several times. The dark red powder was identified as Zn^{II}/**2Z** (75–85 % yield). IR (KBr pellet): $\tilde{\nu} = 1618$s, 1588s, 1466m, 1421m, 1327w, 1234m, 1171s, 1025m, 995w. 954m, 855w, 793m, 746m, 655w cm^{-1}; elemental analysis calcd (%) for Zn^{II}/**2Z**·2 DMSO: C 38.29, H 2.68, N 7.44; found: C 38.85, H 3.26, N 6.86. There are inherent difficulties in formulating the exact number of solvent and other guest molecules in the particles. Zn^{II}/**2E** was obtained by a similar procedure to Zn^{II}/**2Z**, except that **2E** was used instead of **2Z** (70 % yield). IR (KBr pellet): $\tilde{\nu} = 1617$s, 1587s, 1467w, 1418m, 1397m, 1325s, 1173m, 1023m, 953m, 851w, 791w, 746w cm^{-1}; elemental analysis calcd for Zn^{II}/**2E**·2 DMSO: C 46.12, H 3.71, N 8.96; found: C 47.85, H 3.45, N 9.12. There are inherent difficulties in formulating the exact number of solvent and other guest molecules in the particles.

Measurements: Steady-state absorption and emission spectra were recorded on a Hitachi (U-3310) spectrophotometer and an Edinburgh (FS920) fluorimeter, respectively. The detailed setup of picosecond dynamical measurements based on the time-correlated single-photon counting technique has been reported previously.[28] Briefly, a mode-locked Ti: sapphire laser (Tsunami, Spectra-Physics) with 80 MHz repetition rate was used as excitation source. This laser beam was directed into a doubling crystal (BBO) to yield an UV beam as a pulsed excitation source. The excitation source of the second harmonic of the femtosecond Ti:sapphire oscillator (82 MHz, Spectra Physics) combined with a pulse picker (NEOS, model N17389) provides a repetition rate of 8 MHz. This modification can avoid the residue of the emission component from the previous excitation pulse, particularly for components with longer fluorescence decay. The resolution of the monochromator in front of the time-correlated single-photon counting system is 1 nm, and that of the polychromator of the ICCD is 0.3 nm. The fluorescence signal was then analyzed by the time-correlated single-photon counting system (SPC-300, Becker & Hickl) and high-speed photodetector module (OT900, Edinburgh) with a monochromator (resolution, 1 nm) specifically allowing the selected wavelength to pass through. After the instrument response functions are recorded, the time decay data are then analyzed by the nonlinear least-squares procedure in combination with the deconvolution method. The sum of the exponential functions thus allows removal of the effect of instrument time broadening and renders a temporal resolution of about 80 ps. The quality of the fitting is judged by several fitting parameters such as χ^2, standard deviations of the time constants, pre-exponential factors, weighted residuals and autocorrelation functions.[29] Global analysis was not adopted since the initial value is needed to start the nonlinear least-squares procedure. The excitation wavelength was 450 nm and the fluorescence lifetimes were monitored for **1Z** or **1E** at 690 nm (see Figures S7 and S8 in the Supporting Information). In addition, within experimental error, the population decay of **1Z** and **1E** also revealed wavelength independence in, for example, CH_2Cl_2 (see Figures S7 and S8 in the Supporting Information). To investigate the possible differences in photoluminescence between **1Z** and **1E** due to the different topologies, these complexes were studied in the confocal mode of a Witec-Alpha scanning near-field optical microscope (Ulm, Germany). A 514 nm Ar^+ laser line (Coherent, Inova, 5W) was used as excitation source throughout the measurements. The photoluminescence was separated from the scattering light of the excitation pulse by a long-pass filter and sent by an optical fiber to the entrance slit of a polychromator (blazed at 520 nm with a resolution of 0.3 nm) coupled with a sensitive charge-coupled detector (CCD, Princeton Instruments, PI-MAX). The CCD was operated in shutter mode, and the measurements were performed with 300 ms exposure time. All spectra were accumulated over an average of 100 scans. The morphology of Zn^{II}/**2Z** and Zn^{II}/**2E** was studied by field-emission SEM/EDX (FE-SEM, JSM-6500F).

Theoretical calculations: All calculations were done with the Gaussian 03 program suite.[30] Based on the optimized structures, the TDB3LYP/6-31G** theoretical level was used to calculate the vertical excitation energies and ground-state thermodynamics. To consider solvation effects (dichloromethane), the results were then combined with the integral equation formalism polarizable continuum model (IEFPCM)[17] implemented in Gaussian 03. Oscillator strengths were deduced from the dipole transition matrix elements (for singlet states only).

Acknowledgements

We thank the National Center for High-Performance Computing of Taiwan for allowing us generous amounts of computing time. This research was supported by a grant from the National Research Council, Taiwan.

[1] a) D. J. Darensbourg, *Chem. Rev.* **2007**, *107*, 2388–2410; b) C. Baleizao, H. Garcia, *Chem. Rev.* **2006**, *106*, 3987–4043; c) T. R. J. Achard, L. A. Clutterbuck, M. North, *Synlett* **2005**, *12*, 1828–1847; d) P. C. Ford, S. Wecksler, *Coord. Chem. Rev.* **2005**, *249*, 1382–1395; e) E. M. McGarrigle, D. G. Gilheany, *Chem. Rev.* **2005**, *105*, 1563–1602; f) N. S. Venkataramanan, G. Kuppuraj, S. Rajagopal, *Coord. Chem. Rev.* **2005**, *249*, 1249–1268; g) P. G. Cozzi, *Chem. Soc. Rev.* **2004**, *33*, 410–421; h) D. J. Ramón, M. Yus, *Angew. Chem.* **2004**, *116*, 286–289; *Angew. Chem. Int. Ed.* **2004**, *43*, 284–287; i) T. P. Yoon, E. N. Jacobsen, *Science* **2003**, *299*, 1691–1693; j) M. Corsi, *Synlett* **2002**, *12*, 2127–2128; k) N. E. Leadbeater, M. Marco, *Chem. Rev.* **2002**, *102*, 3217–3274; l) M. Bandini, P. G. Cozzi, A. Umani-Ronchi, *Chem. Commun.* **2002**, 919–927; m) G. Musie, M. Wei, B. Subramaniam, D. H. Busch, *Coord. Chem. Rev.* **2001**, *219*, 789–820; n) D. A. Atwood, M. J. Harvey, *Chem. Rev.* **2001**, *101*, 37–52; o) S. Yamada, *Coord. Chem. Rev.* **1999**, *190*, 537–555; p) E. N. Jacobsen, *Acc. Chem. Res.* **2000**, *33*, 421–431; q) H. Shitama, T. Katsuki, *Chem. Eur. J.* **2007**, *13*, 4849–4858; r) N. Nomura, R. Ishii, Y. Yamamoto, T. Kondo, *Chem. Eur. J.* **2007**, *13*, 4433–4451; s) H. Sellner, J. K. Karjalainen, D. Seebach, *Chem. Eur. J.* **2001**, *7*, 2873–2887.

[2] a) E. N. Jacobsen in *Catalytic Asymmetric Synthesis* (Ed.: I. Ojima), Wiley-VCH, New York, **1993**, p. 159–202; b) L. Canali, D. C. Sherrington, *Chem. Soc. Rev.* **1999**, *28*, 85–93; c) C. Yu, X. Dai, W. Su, *Synlett* **2007**, *4*, 646–648; d) H. Yang, J. Li, J. Yang, Z. Liu, Q. Yang, C. Li, *Chem. Commun.* **2007**, 1086–1088; e) M. D. Zhou, J. Zhao, J. Li, S. Yue, C. N. Bao, J. Mink, S. L. Zang, F. E. Kühn, *Chem. Eur. J.* **2007**, *13*, 158–166; f) Z. Zhou, Z. Li, Q. Wang, B. Liu, K. Li, G. Zhao, Q. Zhou, C. Tang, *J. Organomet. Chem.* **2006**, *691*, 5790–5797; g) A. Martinez, C. Hemmert, C. Loup, G. Barré, B. Meunier, *J. Org. Chem.* **2006**, *71*, 1449–1457; h) T. L. Church, Y. D. Y. L. Getzler, G. W. Coates, *J. Am. Chem. Soc.* **2006**, *128*, 10125–10133; i) X. B. Lu, L. Shi, Y. M. Wang, R. Zhang, Y. J. Zhang, X. J. Peng, Z. C. Zhang, B. Li, *J. Am. Chem. Soc.* **2006**, *128*, 1664–1674; j) J. P. Collman, L. Zeng, J. I. Brauman, *Inorg. Chem.* **2004**, *43*, 2672–2679; k) L. Troisi, C. Granito, C. Carlucci, F. Bona, S. Florio, *Eur. J. Org. Chem.* **2006**, 775–781; l) A. L. Williams, J. N. Johnston, *J. Am. Chem. Soc.* **2004**, *126*, 1612–1613; m) J. L. Liang, X. Q. Yu, C. M. Che, *Chem. Commun.* **2002**, 124–125; n) C. J. Sanders, K. M. Gillespie, D. Bell, P. Scott, *J. Am. Chem. Soc.* **2000**, *122*, 7132–7133.

[3] a) H. Y. Shrivastava, M. Kanthimathi, B. U. Nair, *Biochem. Biophys. Res. Commun.* **1999**, *265*, 311–314; b) K. I. Ansari, J. D. Grant, G. A. Woldemariam, S. Kasiri, S. S. Mandal, *Org. Biomol. Chem.* **2009**, *7*, 926–932; c) B. Peng, W. H. Zhou, L. Yan, H. W. Liu, L. Zhu, *Transition Met. Chem.* **2009**, *34*, 231–237.

[4] C. C. Kwok, S. C. Yu, I. H. T. Sham, C. M. Che, *Chem. Commun.* **2004**, 2758–2759.

[5] J. Gradinaru, A. Forni, V. Druta, F. Tessore, S. Zecchin, S. Quici, N. Garbalau, *Inorg. Chem.* **2007**, *46*, 884–895.

[6] a) Y. Lu, F. Hasegawa, T. Goto, S. Ohkuma, S. Fukuhara, Y. Kawazu, K. Totani, T. Yamashita, T. Watanabe, *J. Mater. Chem.* **2004**, *14*, 75–80; b) Y. Lu, F. Hasegawa, S. Ohkuma, T. Goto, S. Fukuhara, Y. Kawazu, K. Totani, T. Yamashita, T. Watanabe, *J. Mater. Chem.* **2004**, *14*, 1391–1395; c) S. Das, A. Nag, D. Goswami, P. K. Bharadwaj, *J. Am. Chem. Soc.* **2006**, *128*, 402–403; d) P. G. Lacroix, *Eur. J. Inorg. Chem.* **2001**, 339–348; e) S. D. Bella, *Chem. Soc. Rev.* **2001**, *30*, 355–366.

[7] P. T. Chou, W. S. Yu, Y. M. Cheng, S. C. Pu, Y. C. Yu, Y. C. Lin, C. H. Huang, C. T. Chen, *J. Phys. Chem. A* **2004**, *108*, 6487–6498.

[8] a) I. Ledoux, J. Zyss, *Pure Appl. Opt.* **1996**, *5*, 603–612; b) P. Wang, Z. Hong, Z. Xie, S. Tong, O. Wong, C. S. Lee, N. Wong, L. Hung, S. Lee, *Chem. Commun.* **2003**, 1664–1665; c) M. Boccia, V. Liuzzo, A. Pucci, P. Narducci, G. Ruggeri, *Macromol. Symp.* **2006**, *235*, 143–151; d) R. Vijayalakshmi, M. Kanthimathi, V. Subramanian, B. U. Nair, *Biochem. Biophys. Res. Commun.* **2000**, *271*, 731–734; e) S. D. Bella, I. Fragala, *New J. Chem.* **2002**, *26*, 285–290.

[9] P. G. Lacroix, S. D. Bella, I. Ledoux, *Chem. Mater.* **1996**, *8*, 541–545.

[10] a) P. Chen, R. Lu, P. Xue, T. Xu, G. Chen, Y. Zhao, *Langmuir* **2009**, *25*, 8395–8399; b) W. Rodríguez-Córdoba, J. S. Zugazagoitia, E. Collado-Fregoso, J. Peon, *J. Phys. Chem. A* **2007**, *111*, 6241–6247; c) S. K. Sahoo, R. K. Bera, M. Baral, B. K. Kanungo, *J. Photochem. Photobiol. A* **2007**, *188*, 298–310; d) W. M. F. Fabian, L. Antonov, D. Nedeltcheva, F. S. Kamounah, P. J. Taylor, *J. Phys. Chem. A* **2004**, *108*, 7603–7612.

[11] a) P. T. Chou, C. H. Huang, S. C. Pu, Y. M. Cheng, Y. H. Liu, Y. Wang, C. T. Chen, *J. Phys. Chem. A* **2004**, *108*, 6452–6454; b) P. T. Chou, P. T. Yu, Y. M. Cheng, S. C. Pu, Y. C. Yu, Y. C. Lin, C. H. Huang, C. T. Chen, *J. Phys. Chem. A* **2004**, *108*, 6487–6498; c) P. T. Chou, S. C. Pu, Y. M. Cheng, W. S. Yu, Y. C. Yu, F. T. Hung, W. P. Hu, *J. Phys. Chem. A* **2005**, *109*, 3777–3787; d) Y. M. Cheng, S. C. Pu, C. J. Hsu, C. H. Lai, P. T. Chou, *ChemPhysChem* **2006**, *7*, 1372–1381; e) C. C. Hsieh, K. Y. Chen, W. T. Hsieh, C. H. Lai, J. Y. Shen, C. M. Jiang, H. S. Duan, P. T. Chou, *ChemPhysChem* **2008**, *9*, 2221–2229.

[12] a) S. Matsumoto, T. Kobayashi, T. Aoyama, T. Wada, *Chem. Commun.* **2003**, 1910–1911; b) S. Matsumoto, K. Shirai, K. Kobayashi, T. Wada, M. Shiro, *Z. Kristallogr.* **2004**, *219*, 239–243; c) T. Kobayashi, S. Matsumoto, T. Tanaka, H. Kunugita, K. Ema, T. Aoyama, T. Wada, *Phys. Chem. Chem. Phys.* **2005**, *7*, 1726–1731; d) T. Kobayashi, S. Matsumoto, T. Aoyama, T. Wada, *Thin Solid Films* **2006**, *509*, 145–148.

[13] D. Y. Yang, Y. S. Chen, P. Y. Kuo, J. T. Lai, C. M. Jiang, C. H. Lai, Y. H. Liao, P. T. Chou, *Org. Lett.* **2007**, *9*, 5287–5290.

[14] a) K. Amimoto, T. Kawato, *J. Photochem. Photobiol. C* **2005**, *6*, 207–226; b) J. Saltiel, E. D. Megarity, *J. Am. Chem. Soc.* **1972**, *94*, 2742–2749; c) J. Saltiel, E. D. Megarity, K. G. Kneipp, *J. Am. Chem. Soc.* **1966**, *88*, 2336–2338; d) J. Saltiel, *J. Am. Chem. Soc.* **1967**, *89*, 1036–1037; e) J. Saltiel, O. C. Zafiriou, E. D. Megarity, A. A. Lamola, *J. Am. Chem. Soc.* **1968**, *90*, 4759–4760; f) J. Saltiel, E. D. Megarity, *J. Am. Chem. Soc.* **1969**, *91*, 1265–1267; g) S. Takeuchi, S. Ruhman, T. Tsuneda, M. Chiba, T. Taketsugu, T. Tahara, *Science* **2008**, *322*, 1073–1077.

[15] a) H. A. Kramers, *Physica* **1940**, *7*, 284–304; b) S. P. Velsko, G. R. Fleming, *Chem. Phys.* **1982**, *65*, 59–70; c) S. P. Velsko, D. H. Waldeck, G. R. Fleming, *J. Chem. Phys.* **1983**, *78*, 249–258.
[16] a) A. D. Becke, *Phys. Rev. A* **1988**, *38*, 3098–3100; b) C. Lee, W. Yang, R. G. Parr, *Phys. Rev. B* **1988**, *37*, 785–789.
[17] M. T. Cances, V. Mennucci, J. Tomasi, *J. Chem. Phys.* **1997**, *107*, 3032–3041.
[18] A. Mitra, L. J. DePue, S. Parkin, D. A. Atwood, *J. Am. Chem. Soc.* **2006**, *128*, 1147–1153.
[19] P. Chen, M. H. Chisholm, J. C. Gallucci, X. Zhang, Z. Zhou, *Inorg. Chem.* **2005**, *44*, 2588–2595.
[20] a) M. Oh, C. A. Mirkin, *Nature* **2005**, *438*, 651–654; b) M. Oh, C. A. Mirkin, *Angew. Chem.* **2006**, *118*, 5618–5620; *Angew. Chem. Int. Ed.* **2006**, *45*, 5492–5494.
[21] W. Lin, W. J. Rieter, K. M. L. Taylor, *Angew. Chem.* **2009**, *121*, 660–668; *Angew. Chem. Int. Ed.* **2009**, *48*, 650–658.
[22] a) R. Kitaura, G. Onoyama, H. Sakamoto, R. Matsuda, S. i. Noro, S. Kitagawa, *Angew. Chem.* **2004**, *116*, 2738–2741; *Angew. Chem. Int. Ed.* **2004**, *43*, 2684–2687; b) N. Hofslokken, L. Skattebol, *Acta Chem. Scand.* **1999**, *53*, 258–262.
[23] a) S. Hagen, P. Kate, M. V. Peters, S. Hecht, M. Wolf, P. Tegeder, *Appl. Phys. A* **2008**, *93*, 253–260; b) S. Hagen, F. Leyssner, D. Nandi, M. Wolf, P. Tegeder, *Chem. Phys. Lett.* **2007**, *444*, 85–90.
[24] a) H. Wei, B. Li, Y. Du, S. Dong, E. Wang, *Chem. Mater.* **2007**, *19*, 2987–2993; b) S. Jung, W. Cho, H. J. Lee, M. Oh, *Angew. Chem.* **2009**, *121*, 1487–1490; *Angew. Chem. Int. Ed.* **2009**, *48*, 1459–1462; c) S. Jung, M. Oh, *Angew. Chem.* **2008**, *120*, 2079–2081; *Angew. Chem. Int. Ed.* **2008**, *47*, 2049–2051; d) W. Cho, H. J. Lee, M. Oh, *J. Am. Chem. Soc.* **2008**, *130*, 16943–16946.
[25] Y. M. Jeon, G. S. Armatas, D. Kim, M. G. Kanatzidis, C. A. Mirkin, *Small* **2009**, *5*, 46–50.
[26] a) T. Rosenfeld, A. Alchalel, M. Ottolenghi, *Photochem. Photobiol.* **1974**, *20*, 121–125; b) Y. Koyama, K. Kubo, M. Komori, H. Yasuda, Y. Mukai, *Photochem. Photobiol.* **1991**, *54*, 433–443; c) Y. Mukai, H. Hashimoto, Y. Koyama, S. Kuroda, Y. Hirata, N. Mataga, *J. Phys. Chem.* **1991**, *95*, 10586–10592; d) Y. Mukai, T. Imahori, Y. Koyama, *Photochem. Photobiol.* **1992**, *56*, 965–975; e) G. Lemercier, M. Alexandre, C. Andraud, I. V. Kityk, *Chem. Phys.* **2004**, *298*, 299–306; f) F. D. Lewis, T. M. Long, *J. Phys. Chem. A* **1998**, *102*, 5327–5332.
[27] L. Ma, C. Abney, W. Lin, *Chem. Soc. Rev.* **2009**, *38*, 1248–1256.
[28] P. T. Chou, Y. C. Chen, W. S. Yu, Y. H. Chou, C. Y. Wei, Y. M. Cheng, *J. Phys. Chem. A* **2001**, *105*, 1731–1740.
[29] *Time-Correlated Single-Photon Counting* (Eds.: D. V. O'Connor, D. Phillips), Academic, New York, **1984**.
[30] Gaussian 03, Revision C. 2, M. J. Frisch, G. W. Trucks, H. B. Schlegel, P. M. W. Gill, B. G. Johnson, M. A. Robb, J. R. Cheeseman, T. Keith, G. A. Petersson, J. A. Montgomery, K. Raghavachari, M. A. Al-Laham, V. G. Zakrzewski, J. V. Ortiz, J. B. Foresman, J. Cioslowski, B. B. Stefanov, A. Nanayakkara, M. Challacombe, C. Y. Peng, P. Y. Ayala, W. Chen, M. W. Wong, J. L. Andres, E. S. Replogle, R. Gomperts, R. L. Martin, D. J. Fox, J. S. Binkley, D. J. Defrees, J. Baker, J. P. Stewart, M. Head-Gordon, C. Gonzalez, and J. A. Pople, Gaussian, Inc., Pittsburgh PA, **2004**.

Received: September 10, 2009
Published online: February 16, 2010

